Available online at www.sciencedirect.com
ScienceDirect
International Journal of Heat and Mass Transfer 51 (2008) 91–103
International Journal of HEAT and MASS TRANSFER
www.elsevier.com/locate/ijhmt

The characteristics and visualization of critical heat flux of R-134a flowing in a vertical annular geometry with spacer grids

Kwi Lim Lee *, In Cheol Bang, Soon Heung Chang

Korea Advanced Institute of Science and Technology, 373-1, Guseong-dong, Yuseong-gu, Daejeon 305-701, Republic of Korea

Received 16 July 2006; received in revised form 13 April 2007
Available online 26 June 2007

Abstract

In the present paper, critical heat flux (CHF) experiments of forced convection boiling were performed to investigate the CHF characteristics of a vertical annular channel with one heated rod and four spacer grids for new refrigerant R-134a. The experiments were conducted under outlet pressure of 11.6, 13, 16 and 20 bar, mass fluxes of 100–600 kg/m^2 s, and inlet temperatures of 25–40 °C. The parametric trend of the CHF data was well consistent with previous understanding in water. The comparison between the present results with effect of the flow obstacle enhancing CHF and water data in similar geometry shows R-134a can be a modeling fluid for simulating water CHF in high pressure and high temperature condition even for annular geometry. The direct observation of flowing bubble behaviors contributes to enhancing our understanding on the effect of flow obstacles for flow boiling heat transfer.

Keywords: R-134a; Flow boiling; CHF; Fluid-to-fluid model; Visualization

1. Introduction

Since industrial revolution of late 18th and early 19th century represented as a boiler, thermal-hydraulic systems using phase change of a fluid or boiling have been steadily studied with considering the economical efficiency of the systems. In particular, the forced convection boiling associated with the change in phase of a fluid and fluid motion driven by an external force is the most preferred heat transfer regime in design of thermal-hydraulic equipments and systems due to its high efficiency of combined latent heat and flow-driven effects. The boiling is faced with the limitation condition called critical heat flux (CHF) that causes an abrupt temperature rise and the physical destruction of the heated surface according to the sudden transition of from efficient wall-liquid zone with nucleate boiling to wall-vapor zone with film boiling.

Therefore, the better understanding of CHF characteristics is very useful and precious for the safety of various high-heat flux thermal-hydraulic systems.

A lot of efforts for experimental and theoretical researches concerning CHF under forced convection boiling have been performed over a few decades. As a result, a lot of models or methods have been developed for prediction of the CHF and its characteristics for various applications [1,2]. Although many aspects of CHF have been understood to some extent, experimental investigations are usually limited to the simplified geometry due to the high expenditure and complexity. Under the absence of a universal CHF correlation commonly usable for various geometries, CHF continue to be studied. Moreover, in recent years, the research activities for the CHF are focused on CHF enhancement techniques to increase the economic efficiency and safety margins of the energy systems. For example, advanced developments of smaller and more powerful electronic devices started to consider dielectric refrigerants with phase changes and refrigeration systems with new refrigerants. In case of nuclear power plant, there is the strong demand of power uprating including new

* Corresponding author. Tel.: +82 42 869 3816.
E-mail addresses: kantavia@kaist.ac.kr, shchang@kaist.ac.kr (K.L. Lee).

0017-9310/$ - see front matter © 2007 Elsevier Ltd. All rights reserved.
doi:10.1016/j.ijheatmasstransfer.2007.04.024

Nomenclature

D	inside diameter (m)
F_G	mass flux index
$F_{\Delta h}$	latent heat index
F_Q	heat flux index
G	mass flux (kg/m^2 s)
G_P	mass flux of prototype fluid (kg/m^2 s)
G_M	mass flux of modeling fluid (kg/m^2 s)
h_{fg}	latent heat (kJ/kg)
Δh_i	inlet subcooling enthalpy (kJ/kg)
L	heated length (m)
Min.	Minimum
P	pressure (bar)
T	temperature (°C)
q_c	critical heat flux (kW/m^2)
q_{co}	q_c for $\Delta h = 0$ (kW/m^2)
x	thermodynamic equilibrium quality

Greek symbols

ρ	density of fluid (kg/m^3)
μ	dynamic viscosity of fluid (Pa/s)
σ	surface tension (N/m)

Subscripts

c	critical
e	hydrodynamic equivalent with D or exit with x
f	saturated liquid
g	saturated vapor
h	heated equivalent with D
M	Modeling fluid
P	Prototype fluid

thermal-hydraulic design due to high-density nuclear fuels. Even in case of nuclear fusion development, plasma-facing components have very high heat flux challenges. Super-critical operation of both coal-burned and nuclear power plants is causing the various thermal-hydraulic issues.

However, due to the high latent heat and high critical pressure of water, direct CHF experiments in water are very expensive and limited in scale. Therefore, if there exists a scaling fluid properly to simulate water boiling phenomena even with low latent heat and low critical pressure, demanded experimental data with the cost of experiments reduced significantly can be acquired. While in heat transfer experiments, various kinds of refrigerants are being used for high temperature and high pressure water scaling, those also have been evaluated to be applicable to CHF experiments [3]. For example, in the development of new nuclear fuel design including various turbulence-generation mixing vanes or flow obstacles, CHF using the refrigerants instead of water has been researched because refrigerant CHF test without high experimental cost is preferred as performance comparison test to select mixing vanes or flow promoter showing the best performance of CHF enhancement among various candidate designs [4].

Among CHF scaling fluids, the refrigerant, R-12 had extensively been used to model the CHF characteristics of water due to its low latent heat, low critical pressure, and well known properties [5]. However, the refrigerants such as R-134a and R-152a have been evaluated as an alternative in modeling CHF in water due to its harmlessness on the environment [6,7] because CFC (clorofluorocarbon) family such as R-12, R-22, R-133, and R-144, could deplete the ozone layer. In particular, since the thermophysical properties of R-134a are close to R-12, R-134a is considered to be a new scaling fluid. Tain and Cheng [6] reported that the CHF test data in R-134a agreed very well with the CHF data predicted by converting the standard CHF look-up table from water to R-134a equivalent condition. Also, Pioro et al. [8] reported that the agreement between the CHF look-up table and the experiment is surprisingly good. However, those studies were confined to simple tube geometry.

In order to investigate R-134a CHF characteristics for various geometries, develop new thermal-hydraulic CHF enhancement techniques and run its performance test, KAIST (Korea Advanced Institute of Science and Technology) built a forced convection boiling CHF loop using R-134a as a working fluid and have been studying since 2001. Up to now, KAIST CHF investigations are on such geometries as rectangular channel [9], uniformly heated vertical tube [10], uniformly heated vertical rifled tubes [11].

In particular, the present work is motivated by the following two concerns: (i) the flow boiling CHF characteristics of R-134a for various geometries are not well-known; (ii) for various geometries, phenomenological characteristics or boiling phenomena remain unexplored. Therefore, this study aims to provide R-134a CHF database with the CHF characteristics and bubble behaviors in a new geometry of vertical annular channel including flow obstacles. This schematic CHF test using R-134a is used to examine the forced convection flow boiling, CHF and the suitability of R-134a as a CHF modeling fluid of water in annular geometry. Also, this CHF data will be used as a reference for future post-CHF studies of R-134a and the visualization of flow boiling will be used for understanding the effect of flow obstacles.

2. Experimental method

2.1. Experimental loop

CHF experiments and visualization have been carried out in the R-134a forced convection boiling CHF loop at

Korea Advanced Institute of Science and Technology (KAIST). It is schematically shown in Fig. 1. The experimental loop consists of a test section, a non-seal canned pump, a Coriolis-type mass flow meter, a preheater for inlet subcooling control, a pressurizer of an accumulator connected to high pressure N_2 gas bottle and venting system for pressure control, a chiller or chilling system consisting of a heat exchanger of R-134a flow chilled with circulation system of water-propylene glycol cooled by R-22 refrigeration system, a condenser cooled by tap water. The loop is filled with R-134a in the vacuum condition made by a vacuum pump. The mass flow rate is controlled by adjustments of the pump rotation speed, bypass valve and two throttling valves. The throttling valves are located at the upstream of the test section inlet to prevent flow fluctuation.

2.2. Test section

A vertical annular channel with one heated rod and four spacer grids is shown in Fig. 2. The test section consists of a body of an inner rectangular flow channel ($D_e = 10.97$ mm, $D_h = 38.90$ mm) of 19×19 mm^2, single heater rod with outer diameter of 9.5 mm in the center of flow channel and visualization windows of two sides. The heater rod consists of sheath or cladding made of Inconel 600 of 1 mm thickness, an electrical insulation layer of MgO which fills between the sheath layer and heating element and spiral-strip heating element which is filled by Al_2O_3. The rod is heated indirectly by 22 kW AC (alternating current) power supply for 1830 mm length. Power shape of the heater rod is uniform throughout the heated section. Four I-types of spacer grids (of rectangular cell) have been used for providing a uniform annular gap for rod and for preventing rod vibration and contact between the rod and the shroud. Three of them are located in the 298, 798, and 1443 mm from the bottom of heated rod. The other one is installed in inlet part for anti-vibration.

To measure the heated wall surface temperature, six K-type thermocouples, whose sheath diameter is 0.5 mm, are embedded in the cladding of the heater rod. The length from the bottom end of heated section to each thermocouple is 920, 1320, 1520, 1720, 1800, and 1820 mm, respectively. For the measurement of fluid temperature, four T-type thermocouples and four pressure taps are installed axially in the annular channel. In particular, for direct observation of characteristic heat transfer phenomena, two visual window sections are installed in the exit part including the last spacer. The visualization of flow pheonomena is performed by a digital camera with a few millions record pixels, close-up lens and high-speed flash with 1/8700 short duration time [9]. Generally, an annular channel for CHF studies is designed as a type of concentric circular inner tube and outer tube, but in the present study, in order to investigate both CHF characteristic and boiling phenomena under a little high pressure conditions with spacer grid installation, rectangular outer channel is adopted instead of outer circular tube. This difference could make a distinction between present data and general annulus CHF data.

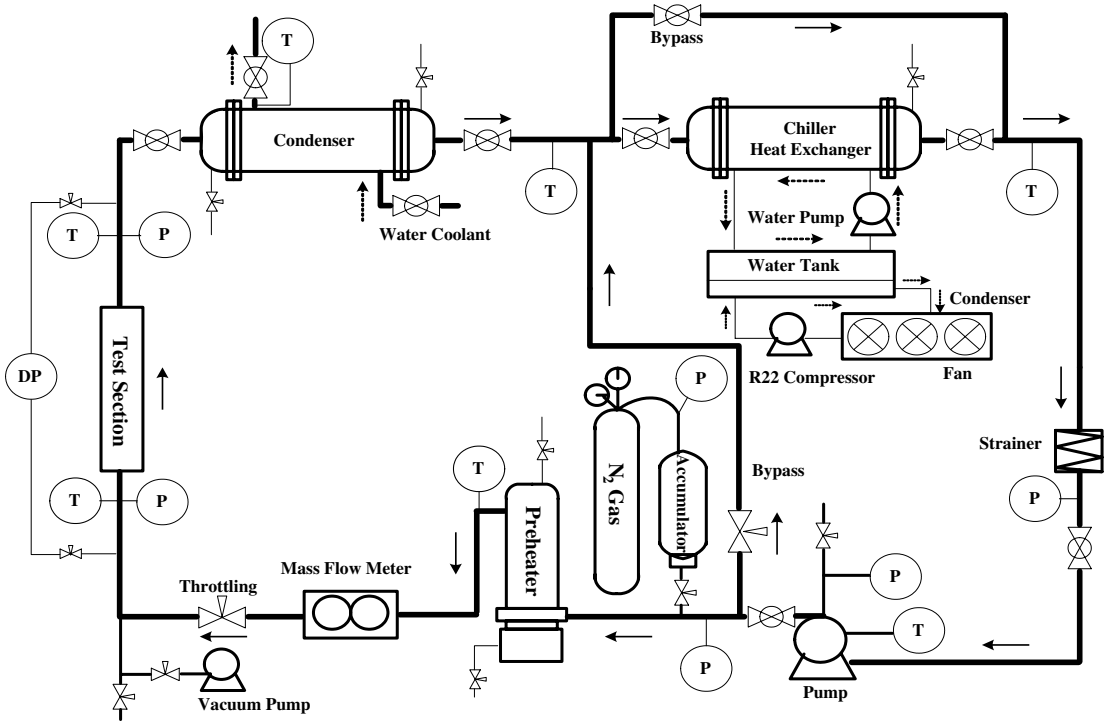

Fig. 1. KAIST R-134a forced convection boiling CHF loop [3].

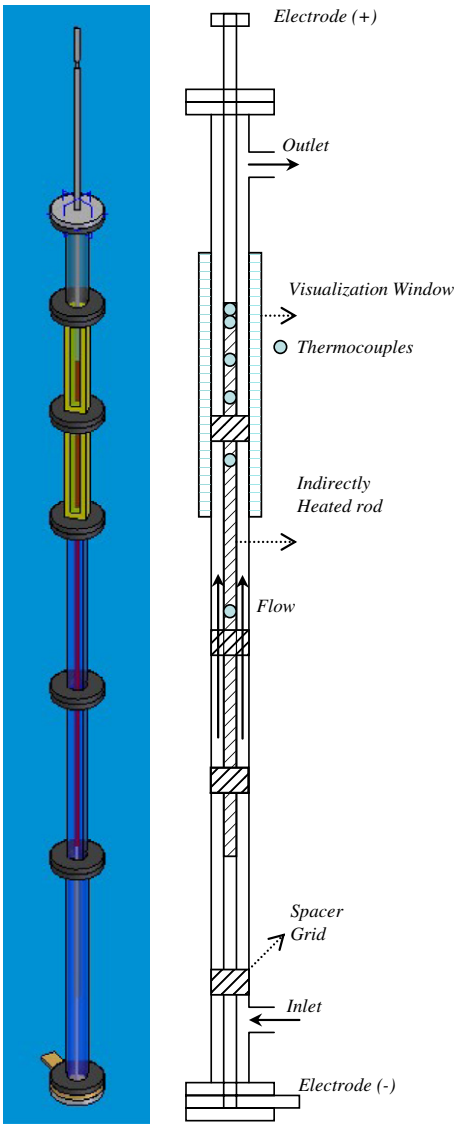

Fig. 2. Schematic diagram of the test section.

2.3. Experimental condition

In the present study the experiment on critical heat flux of R-134a was performed for the refrigerant mass flux varying from 100 to 600 kg/m^2 s, the pressure of 11.6, 13, 16, and 20 bar and the subcooling temperature from 23 to 40 °C. Table 1 shows the test condition. The uncertainties of the measurement parameters are analyzed by the error propagation method [17]. The uncertainties of the applied heat flux and mass flux were less than ±2.5% and ±2.0%, respectively. The heat balance tests are conducted to estimate heat loss resulting in negligible loss. Uncertainties for the pressure and fluid temperature measurements are ±9 kPa and ±0.5 °C.

Table 1
Test condition

Experimental parameter	Experimental condition
Pressure (bar)	11.6, 13, 16, 20
Mass flux (kg/m^2 s)	100–600
T_{in} (°C)	23–40
Locations of K-type thermocouples (mm)	920, 1320, 1520, 1720, 1800, 1820
Heated length (mm)	1830

3. Experimental results and discussion

3.1. Characteristics of CHF data

The results of the present works represent the characteristics of the flow boiling heat transfer for R-134a in an annular channel by measuring the critical heat flux. The 96 CHF data measured in the study are tabulated in Table 3 for future use by those who will develop prediction methods or design a R-134a based system. The CHF in forced convective boiling, generally, is a function of the channel geometry, flow conditions and heat flux distributions (uniform or non-uniform heating conditions). For the parametric trends of the CHF in flow boiling of the case where the subcooled R-134a is injected into the bottom of uniformly-heated, vertical annular channel, the CHF is a function of six independent variables, i.e., system pressure (P), heated length (L_h), tube diameter (D_i), flow channel width (w), mass flux (G), and inlet subcooling (Δh_i). This relationship represents the inlet conditions concept, and inlet temperature (T_{in}) or inlet quality (x_i) can be used instead of inlet subcooling. In the exit condition concept, exit quality (x_e) is used instead of inlet subcooling. Exit quality and inlet subcooling are related to each other via the heat balance equation. The quality is the thermodynamic equilibrium quality at the test section outlet, which was calculated by assuming the following steady-state heat balance equation:

$$x_e = \frac{h - h_f}{h_{fg}} = \frac{4\pi D_i L_h q}{(4w^2 - \pi D_i^2) G h_{fg}} - \frac{\Delta h_i}{h_{fg}} \quad (1)$$

Generally, for the prediction of the CHF, it is common to adopt the local conditions hypothesis that neglects the length effect on the CHF [3]. The critical quality (local quality at CHF occurrence location), x_c, is used instead of exit quality, x_e, because it is possible to generalize the relationship even for the non-uniform axial heat flux distributions. Under the present fixed conditions of heated length (L_h), tube diameter (D_i), flow channel width (w) and uniform heating condition of the heater, finally, CHF is the following type of function:

$$q_c = f(P, G, x_c) \text{ or } q_c = f(P, G, \Delta h_i) \quad (2)$$

Therefore, here, the parametric trend of R-134a CHF data is analyzed with respect to the critical quality, or the exit quality at CHF occurrence, mass flux, pressure, and inlet subcooling. The overall behavior of the CHF and such critical quality are shown in Fig. 3. The parametric trend of the quality and mass flux is also shown in Fig. 4. With the quality increasing, CHF is decreased like typical water

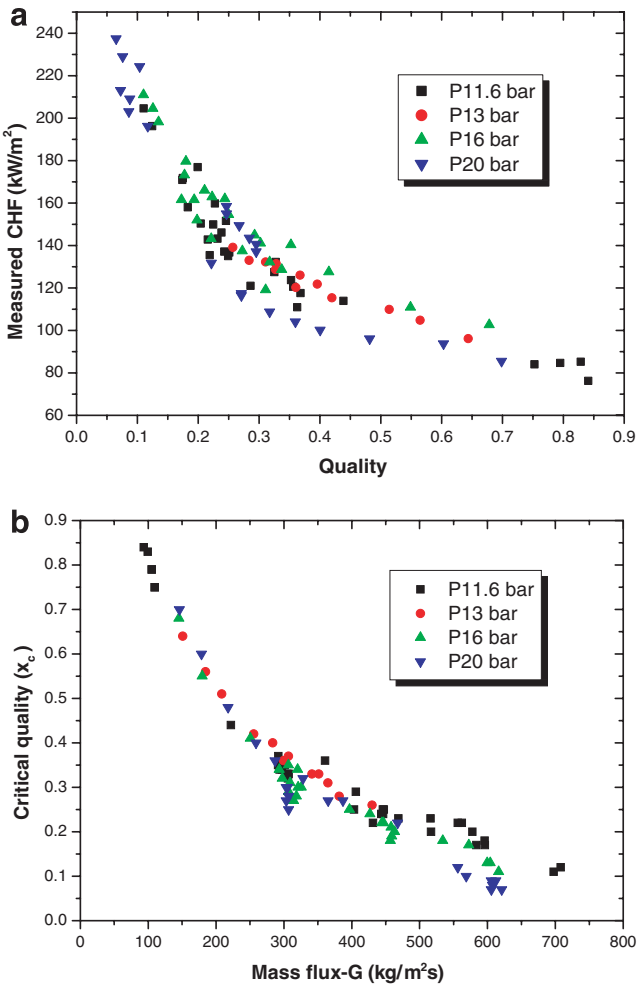

Fig. 3. Parametric trend of (a): CHF with respect to critical quality x_c, (b) critical quality, x_c with respect to mass flux, G for R-134a in annular channel.

CHF trend. As mass flux approaches to a low value, the quality is increased. In particular, Figs. 4 and 5 show pressure effect on CHF with the inlet subcooling change on the CHF of R-134a in annular channel. Higher pressure is causing the lower CHF at same inlet subcooling. Figs. 6–8 show mass flux effect on CHF in fixed pressures of 11.6, 16, and 20 bar, respectively, with inlet subcooling change. In each pressure, the CHF has the parametric trend of its increase with increasing mass flux. These trends show good agreements with the general understanding in the water. In addition, the correlations for Eq. (2) types based on the present CHF data are proposed as follows:

$$q_c = 132.0687P^{-0.0982}G^{-0.0505}x_c^{-0.4667} \quad (3)$$

$$q_c = 6.713P^{-0.173}G^{0.4143}\Delta h_i^{0.3148} \quad (4)$$

Fig. 9 shows the comparison of the experimental CHF data with the proposed correlations (3) and (4) based on inlet subcooling and critical quality, respectively. The average errors and RMS errors of the predictions are 0.124%, 0.29% and 4.0%, 7.9%, respectively.

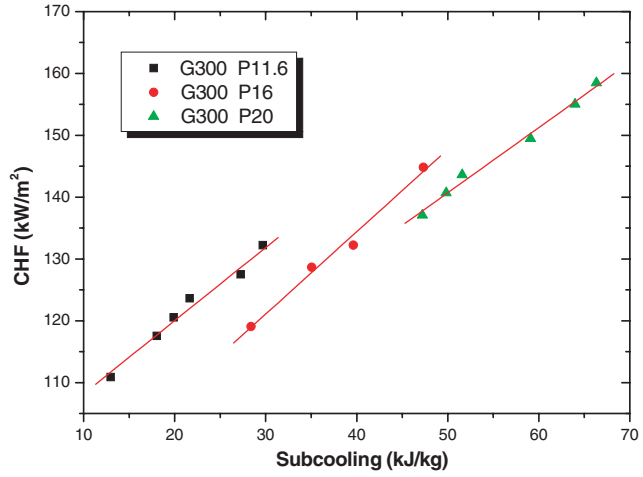

Fig. 4. Effect of inlet subcooling enthalpy at different pressures on CHF of R-134a in annular channel ($G = 300$ kg/m^2 s).

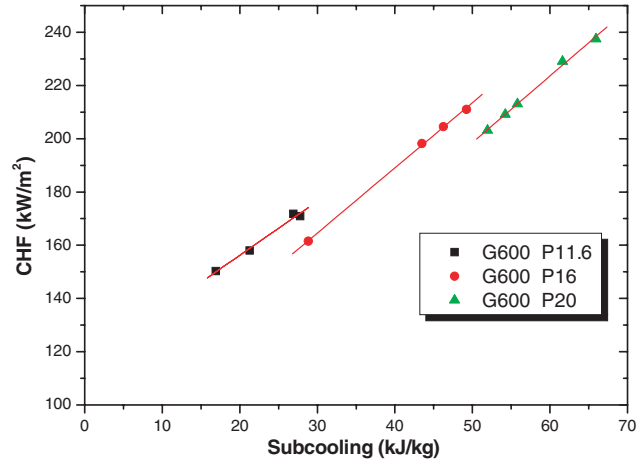

Fig. 5. Effect of inlet subcooling enthalpy at different pressures on CHF of R-134a in annular channel ($G = 600$ kg/m^2 s).

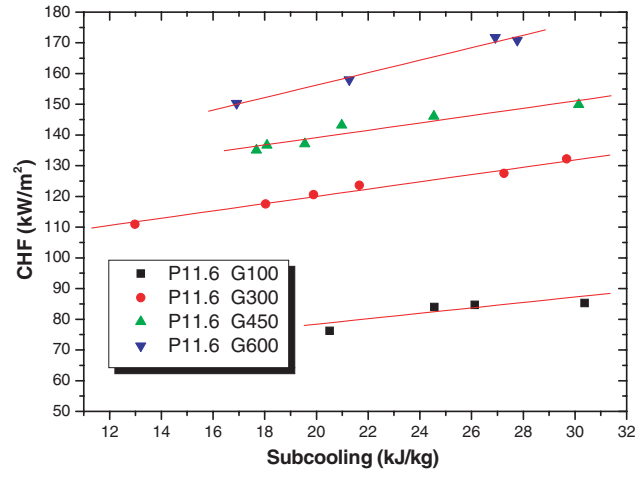

Fig. 6. Effect of inlet subcooling for different pressure on CHF of R-134a in annular channel.

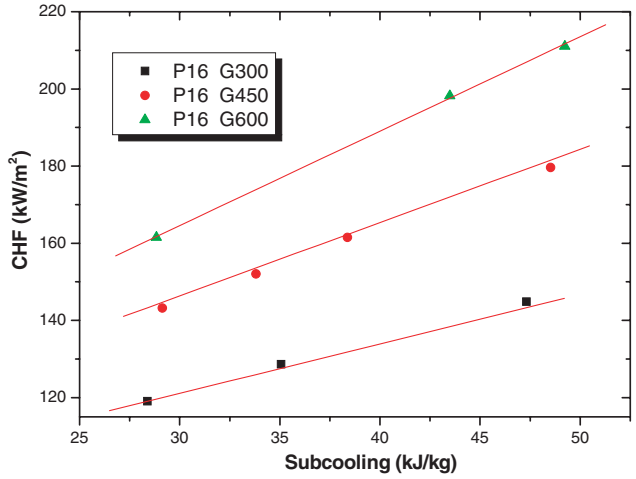

Fig. 7. Effect of inlet subcooling for different mass flux on CHF of R-134a in annular channel.

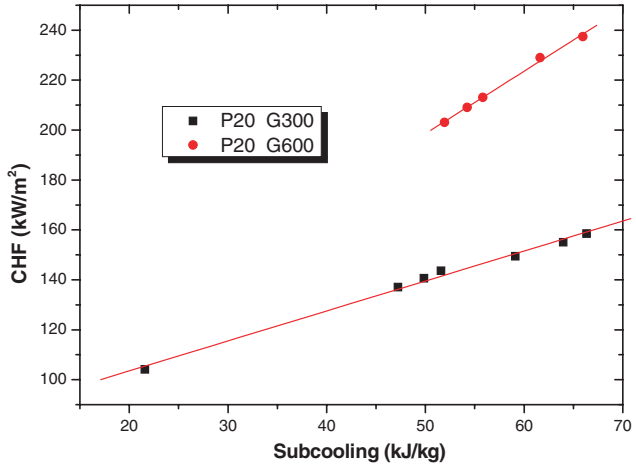

Fig. 8. Effect of inlet subcooling for different mass flux on CHF of R-134a in annular channel.

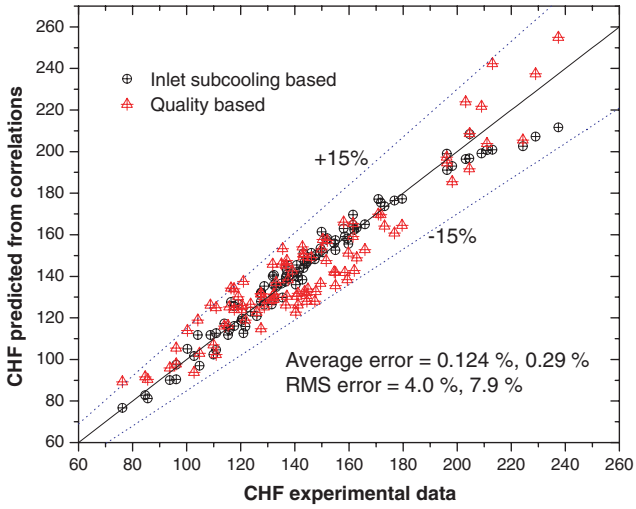

Fig. 9. Comparison of test results with the proposed correlations.

3.2. Fluid-to-fluid scaling

The present study includes the CHF data related to fluid-to-fluid modeling to evaluate the possibility of using the CHF data obtained from R-134a in annular channel for CHF prediction of water. Fluid-to-fluid modeling of critical heat flux is to simulate the CHF behaviors for water by employing other useful modeling fluids [6].

Among the efforts to find out a proper fluid-to-fluid scaling law, Ahmad's [7] model is widely used. Based on dimensional analysis according to conventional Pi Theorem, he derived the following non-dimensional parameter groups showing CHF behavior:

$$\frac{q_c}{Gh_{fg}} = f\left(\frac{L_h}{D}, \frac{\rho_f}{\rho_g}, \frac{\Delta h_i}{h_{fg}}, \frac{\mu_f}{\mu_g}, \frac{\mu_f^2}{\sigma D \rho_f}, \frac{GD}{\mu_f}\right) \tag{5}$$

The LHS (left-hand side) is CHF shown as Boiling Number. As all non-dimensional parameter groups cannot be made equally in real condition, generally geometric, hydrodynamic and thermodynamic similarities are first fitted for the fluid-to-fluid scaling [3].

Geometric similarity:

$$\left[\frac{L_h}{D}\right]_P = \left[\frac{L_h}{D}\right]_M \tag{6}$$

Hydrodynamic similarity:

$$\left[\frac{\rho_f}{\rho_g}\right]_P = \left[\frac{\rho_f}{\rho_g}\right]_M \tag{7}$$

Thermodynamic similarity:

$$\left[\frac{\Delta h}{h_{fg}}\right]_P = \left[\frac{\Delta h}{h_{fg}}\right]_M \tag{8}$$

As it is almost impossible to make the individual parameter groups for the others be equal among scaling fluids, three parameters in RHS (right hand side) of Eq. (3) are combined into one scaling parameter. The present study uses the Katto's model widely used for a scaling law and is expressed as follows:

$$\left[\frac{G\sqrt{D}}{\sqrt{\sigma\rho_f}}\right]_P = \left[\frac{G\sqrt{D}}{\sqrt{\sigma\rho_f}}\right]_M \tag{9}$$

The following procedures can be used to convert the R-134a CHF data from the scaling fluid to the water CHF data [3,10].

(a) Calculate the density ratio of the liquid to the vapor. Find the pressure where the density ratio is same.
(b) Calculate the mass ratio at the equivalent pressure as follows:

$$F_G = \frac{G_P}{G_M} = \frac{\left(\sqrt{\sigma\rho/D}\right)_P}{\left(\sqrt{\sigma\rho/D}\right)_M} \quad (10)$$

(c) Calculate the latent scaling ratio defined as latent ratio of prototype fluid to vapor of model fluid as follows:

$$F_{\Delta h} = \frac{(h_{fg})_P}{(h_{fg})_M} \quad (11)$$

(d) Calculate the heat flux scaling ratio by multiplying the latent scaling ratio and the heat flux scaling ratio as follows:

$$F_Q = F_G \times F_{\Delta h} \quad (12)$$

(e) Calculate the critical heat flux from the heat flux scaling ratio as follows:

$$(q_c)_P = F_Q \times (q_c)_M \quad (13)$$

3.2.1. Comparison of CHF data of R-134a and water by using the fluid-to-fluid model

In this section, R-134a CHF tests were performed in corresponding condition acquired according to above-mentioned procedures for the CHF experimental data of water which was obtained in concentric annular channel of the outer diameter of 19.4 mm without grid by Chun et al. [15,12]. The experimental condition is summarized in Table 2. The tested mass fluxes range from 145 to 470 kg/m^2 s and operating pressures range from 13 to 20 bar.

Fig. 10 with overall parametric trend of CHF vs mass flux shows the comparison results between the measured R-134a CHF data which are converted to water equivalent conditions and the predicted data converted from Chun's water CHF data. The results indicate the possibility of R-134a as the modeling fluid of water. Experimental results in Fig. 11a–c show the differences between CHF data for water and R-134a data with respect to mass flux at fixed pressure and subcooling conditions of 13 bar (21 kJ/kg), 16 bar (37 kJ/kg), and 20 bar (22 kJ/kg).

The comparison of CHF results as shown in Fig. 12 shows that the measured CHF are about 1.5 times as high as the predicted CHF with very similar parametric trends for each figure. Such higher values of R-134a CHF data for nearly all test conditions seems to be due to out-boundary rectangular geometry and spacer grids. The experimented R-134a test section is one rod bundle rectangular

Table 2
Test matrix condition of R-134a for fluid to fluid modeling

Pressure (bar)	T_{in} (°C)	Mass flux (kg/m^2 s)						
13	35	151	185	208	255	306	381	430
16	33	145	180		251	326	397	458
20	54	146	179	217	259	328	387	468

Table 3
Table of measured CHF data

P	G	Δh_i	q''_c (kW)	x_c
11.60	100	20.51	76.23	0.84
11.60	100	26.12	84.66	0.79
11.60	100	26.12	84.66	0.79
11.60	222	27.68	113.88	0.44
11.60	300	32.48	136.68	0.35
11.60	300	18.03	117.57	0.37
11.60	300	38.39	144.47	0.34
11.60	300	34.44	141.16	0.35
11.60	300	39.22	147.39	0.34
11.60	300	12.98	110.91	0.36
11.60	300	19.89	120.56	0.36
11.60	300	21.66	123.62	0.35
11.60	300	37.58	144.31	0.33
11.60	300	40.90	147.8	0.32
11.60	300	27.25	127.50	0.33
11.60	300	27.25	127.50	0.33
11.60	300	29.68	132.24	0.33
11.60	403	32.25	151.61	0.25
11.60	406	11.00	120.96	0.29
11.60	450	30.15	149.89	0.22
11.60	450	24.54	146.10	0.24
11.60	450	18.09	136.66	0.25
11.60	450	19.55	137.06	0.24
11.60	450	17.68	135.04	0.25
11.60	450	20.98	143.20	0.23
11.60	516	22.40	159.77	0.23
11.60	516	33.38	176.85	0.20
11.60	556	11.41	135.44	0.22
11.60	562	13.81	142.77	0.22
11.60	600	16.91	150.31	0.20
11.60	600	27.77	170.90	0.17
11.60	600	21.27	158.03	0.18
11.60	600	26.92	171.79	0.17
11.60	700	38.00	204.57	0.11
11.60	700	32.77	196.22	0.12
13.00	150	21.46	96.16	0.64
13.00	185	20.54	104.78	0.56
13.00	208	20.78	109.84	0.51
13.00	255	21.06	115.34	0.42
13.00	284	20.52	121.73	0.40
13.00	300	20.59	120.22	0.36
13.00	307	21.22	125.96	0.37
13.00	341	21.21	128.69	0.33
13.00	351	20.48	131.46	0.33
13.00	365	20.96	132.25	0.31
13.00	381	22.53	133.05	0.28
13.00	430	21.71	139.10	0.26
16.00	145	36.53	102.70	0.68
16.00	180	38.4	110.92	0.55
16.00	250	37.14	127.51	0.41
16.00	300	35.06	128.67	0.34
16.00	300	39.63	132.23	0.32
16.00	300	35.65	140.31	0.35
16.00	300	47.32	144.84	0.29
16.00	300	28.38	119.06	0.31
16.00	300	57.53	159.38	0.27
16.00	300	43.97	137.45	0.27
16.00	300	51.3	155.04	0.28
16.00	300	20.48	115.73	0.34
16.00	300	32.03	127.53	0.30
16.00	300	38.78	141.13	0.30
16.00	397	38.02	154.58	0.25
16.00	450	36.66	161.96	0.24

(continued on next page)

Table 3 (*continued*)

P	G	Δh_i	q''_c (kW)	x_c
16.00	450	37.38	162.87	0.22
16.00	450	29.13	143.20	0.22
16.00	450	48.52	179.63	0.18
16.00	450	38.61	165.96	0.21
16.00	450	38.38	161.54	0.19
16.00	450	33.81	152.02	0.20
16.00	534	36.31	173.17	0.18
16.00	600	28.84	161.54	0.17
16.00	600	43.49	198.18	0.13
16.00	600	46.24	204.55	0.13
16.00	600	49.23	211.03	0.11
20.00	146	20.2	85.60	0.70
20.00	179	21.52	93.78	0.60
20.00	218	21.32	96.15	0.48
20.00	259	21.57	100.26	0.40
20.00	300	21.58	104.10	0.36
20.00	300	59.1	149.48	0.27
20.00	300	49.84	140.66	0.30
20.00	300	47.23	137.06	0.30
20.00	300	66.34	158.49	0.25
20.00	300	63.97	155.03	0.25
20.00	300	51.58	143.61	0.28
20.00	300	21.56	108.75	0.32
20.00	365	25.37	116.44	0.27
20.00	387	22.36	117.48	0.27
20.00	468	24.67	131.81	0.22
20.00	556	52.66	196.27	0.12
20.00	569	61.47	224.34	0.10
20.00	600	65.94	237.48	0.07
20.00	600	54.24	209.06	0.09
20.00	600	61.61	229.02	0.08
20.00	600	51.94	203.11	0.09
20.00	600	55.81	213.07	0.07

shape with four spacer grids in location of the inlet part and 289, 798, and 1443 mm from the bottom of heated rod, but the water test section is concentric annular circular channel of the outer diameter of 19.4 mm ($D_e = 9.9$ mm, $D_h = 30.12$ mm) without any grid.

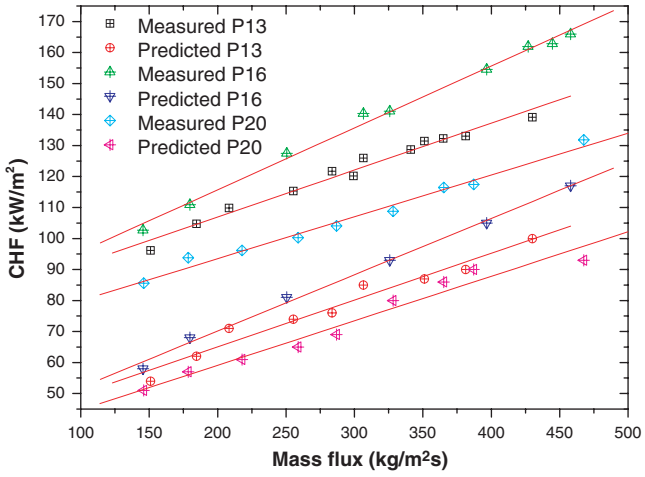

Fig. 10. The comparison between CHF data of R-134a (measured) and R-134a equivalent water data (predicted) in annular flow.

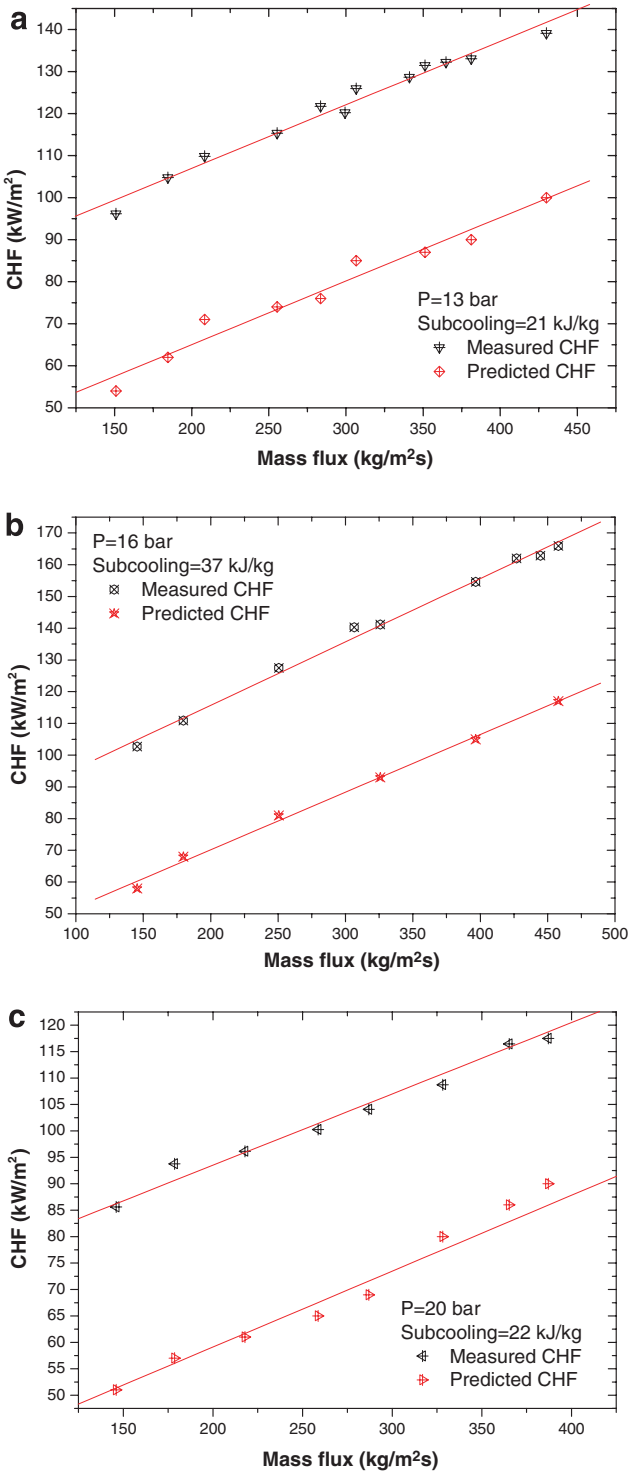

Fig. 11. Comparison of CHF data of R-134a (measured) and R-134a equivalent water data (predicted) in (a) 13 bar, 21 kJ/kg, (b) 16 bar, 37 kJ/kg, and (c) 20 bar, 22 kJ/kg.

3.2.2. Comparison existing CHF correlations

Previous section shows the direct comparison of experimental data of water and R-134a in similar geometry. In addition, in the present study, it is simply tried to compare with R-134a CHF data indirectly by using well-known tube correlations such as Bowring [13] and Katto and Ohno [14]

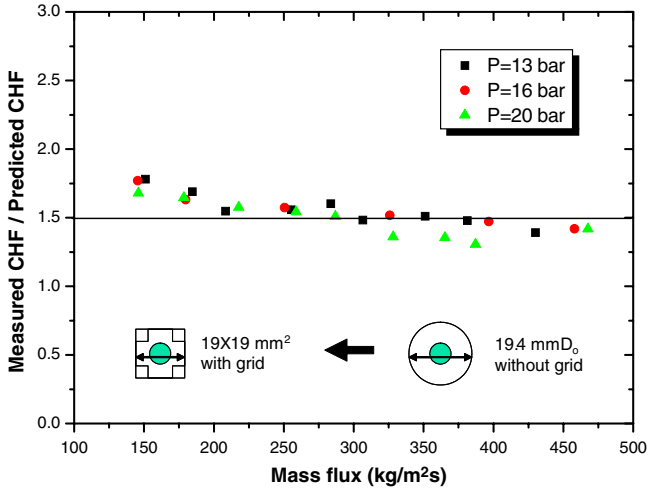

Fig. 12. Comparison of CHF data of R-134a (measured) and R-134a-equivalent CHF data of water (predicted).

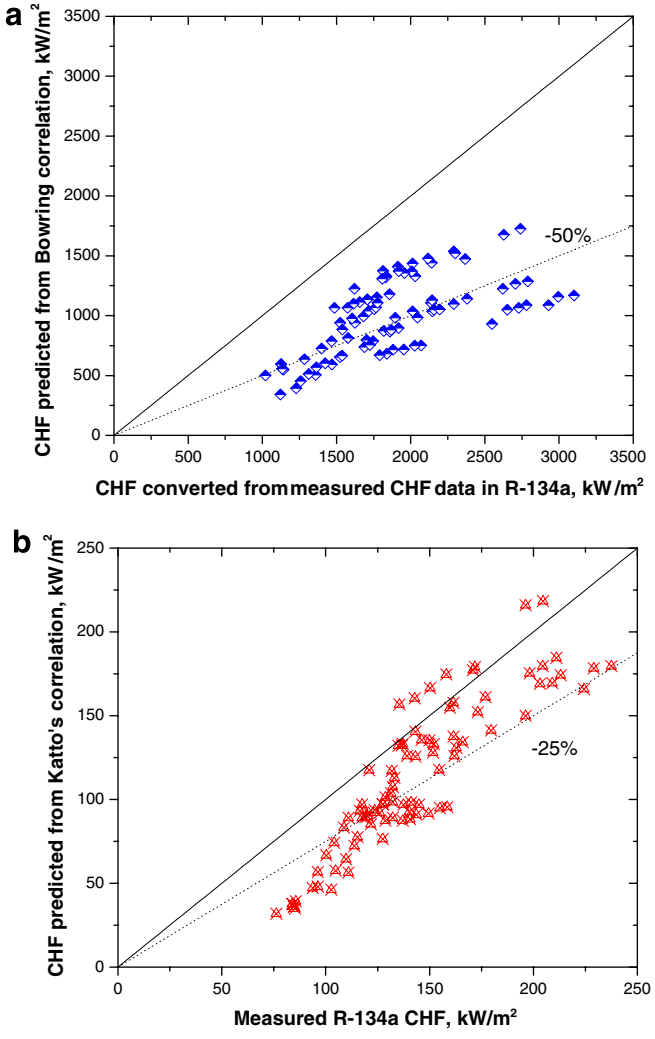

Fig. 13. Comparison of test results in annular channel with Bowring's and Kotto's correlations.

because already it is well shown that the correlations predicted with good agreements with R-134a tube data in Kim and Chang [10]'s tube geometry study.

3.2.2.1. Bowring's prediction method. The correlation of Bowing was developed for CHF in water and based on the inlet condition [13]. The correlation is

$$q_c = \frac{A' + 0.25DG\Delta h_i}{C' + L} \tag{14}$$

where $A' = \frac{0.5792 h_{fg} DGF_1}{1+0.0143F_2D^{0.5}G}$, $C' = \frac{0.077F_3DG}{1+0.347F_4(G/1356)^n}$.

F_1, F_2, F_3, F_4 and n are the function of a non-dimensional pressure, $P' = P/68.95$.

$$n = 2 - 0.5P' \tag{15}$$

$$F_1 = P'^{-0.368}\exp[0.648(1-P')] \tag{16}$$

$$F_1/F_2 = P'^{-0.448}\exp[0.245(1-P')] \tag{17}$$

$$F_3 = P'^{0.219} \tag{18}$$

$$F_4 = F_3P'^{1.649} \tag{19}$$

The correlation of Bowring is applicable for the pressure of 2–190 bar, tube diameter of 2–45 mm, tube length 0.15–3.7 m and mass flux of 136–18,600 kg/m^2 s. Since this correlation is applicable for only water, the present CHF data of R-134a in annular geometry are first converted into water-equivalent values using the correlations of scaling indices developed for water-to-R-134a modeling. Fig. 13a shows the comparison of the water-equivalent CHF data converted from the CHF data in R-134a with the CHF prediction using Bowring correlation with hydraulic equivalent diameter of annular geometry. The average error and RMS error of the prediction are −46.5% and 48.3%, respectively.

3.2.2.2. Katto's prediction method. Katto and Ohno presented the improved version of generalized CHF correlation of forced convective boiling in uniformly heated tubes covering various fluids based on the inlet condition [14]. The basic equation for CHF is:

$$q_c = q_{co}\left(1 + K\frac{\Delta h_i}{h_{fg}}\right) \tag{20}$$

Since the density ratio of vapor to liquid is less than 0.15 for the testing pressure range of this study, q_{co} is obtained from the minimum value as follows:

$$\frac{q_{co}}{Gh_{fg}} = \text{Min.}\left[\frac{CW^{0.043}}{L/D}, \frac{0.1(\rho_g/\rho_f)^{0.133}W^{1/3}}{1+0.0031(L/D)}, \frac{0.098(\rho_g/\rho_f)^{0.133}W^{0.433}(L/D)^{0.27}}{1+0.0031(L/D)}\right] \tag{21}$$

The non-dimensional parameter, K is obtained from the minimum values as follows:

$$K = \text{Min.}\left[\frac{0.261}{C(\sigma\rho_f/G^2L)^{0.043}}, \frac{(5/6)(0.0124 + D/L)}{(\rho_g/\rho_f)^{0.133}W^{1/3}}\right] \tag{22}$$

where $W = \frac{\sigma\rho_f}{G^2L}$ and $C = 0.34$.

Fig. 13b shows the comparison of CHF test data in R-134a with the CHF data obtained by using the generalized correlation of Katto. The average error and RMS error of the prediction are −23% and 29.2%, respectively.

Both correlations show reasonable agreements but show a shift of distribution with around −50%, in particular, 29.2% RMS error in Katto's generalized correlation. This trend indirectly shows the effect of spacer grid in annular geometry as directly compared in the previous section because the hydraulic diameter is used. In addition, it plausibly describe the possibility of general annulus correlations can be made with the correction factor of spacer grid.

4. Direct observation of flow boiling phenomena

In the present work, the direct observation of flowing bubble behaviors contributes to enhancing our understanding not only on flow boiling heat transfer phenomena, but also on the effect of flow obstacles for flow boiling heat transfer contributing in advanced development for heat transfer enhancement devices. The observations for R-134a flow boiling phenomena have been reported just for horizontal annular duct under relatively lower heat flux conditions [16,17] and for rectangular channel to CHF conditions [9]. Lie and Lin's [16,17] flow visualization shows that the mean diameter of the bubbles departing from the heating surface decreases slightly at increasing R-134a mass flux and moreover, the bubble departure frequency increases at reducing duct size mainly due to the rising shear stress of the liquid flow. Bang et al. [9] examined the behavior of near-wall bubbles in subcooled flow boiling of water and R-134a in a vertical rectangular channel and described the coalescence of the bubbles. The bubbles were found to be smaller at a higher mass flux.

For the vertical annular channel as a new geometry showing R-134a characteristics, the present visualization work was performed at the downstream of test section with visualization windows for observations of the characteristic flow pattern including bubble generations and bubble flow from lower heat flux to higher heat flux near a CHF condition along with heated channel, including a grid region. Generally, flow pattern near CHF condition in annular geometry at low mass flux has a film-splitting structure of inner liquid film on heated surface and outer liquid film

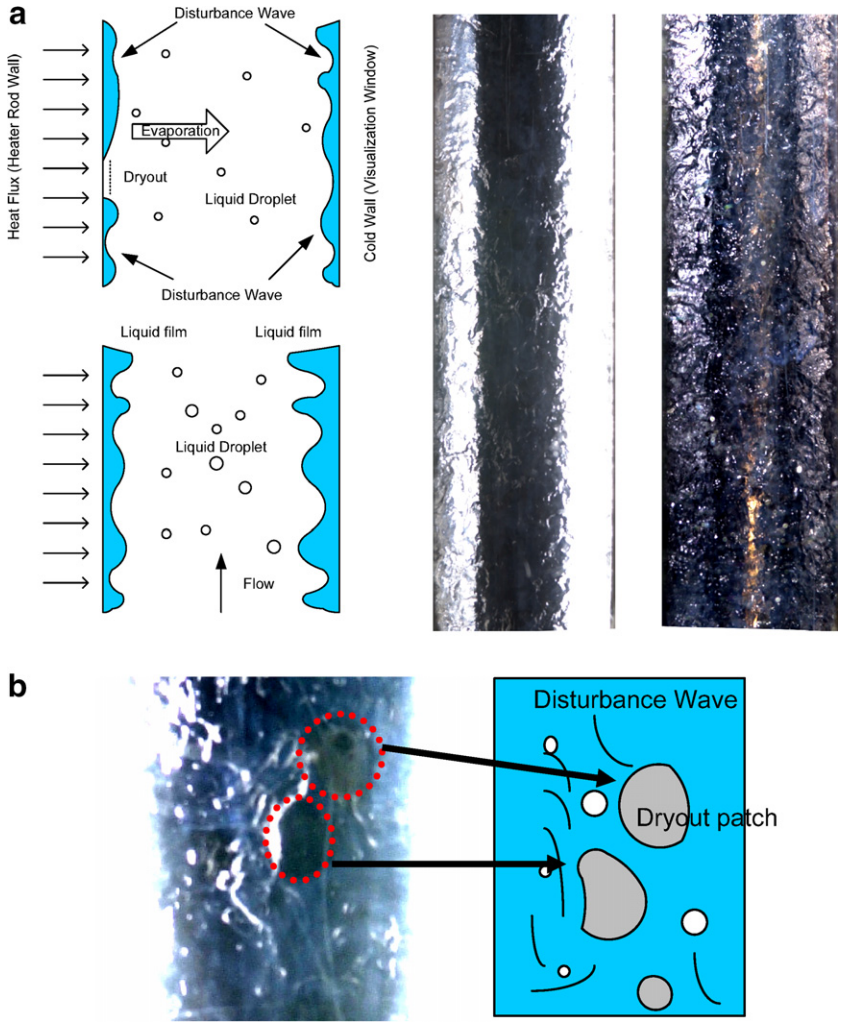

Fig. 14. Observation of near-CHF phenomena: (a) liquid film-splitting structure of annular geometry and observation of developing CHF condition ($P = 11.6$ bar, $G = 100$ kg/m^2, ~90% CHF) and (b) appearance of local dryout patch on inner liquid film.

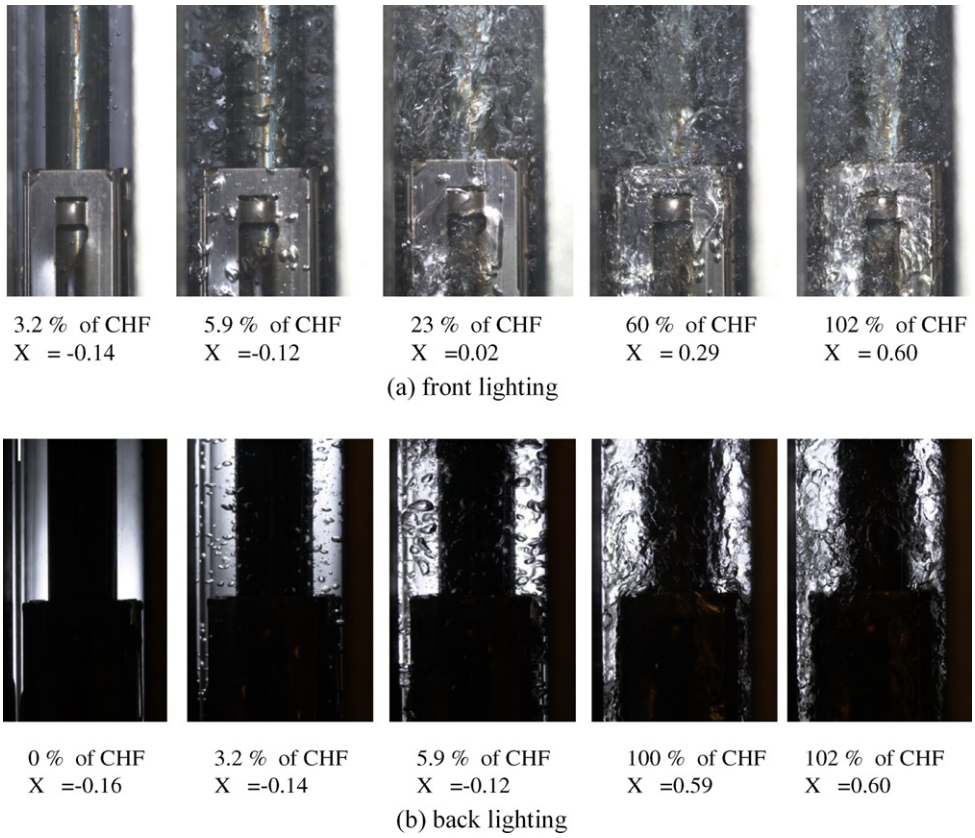

Fig. 15. Flow pattern change with heat flux increasing at downstream of spacer grid ($P = 11.6$ bar, $G = 100$ kg/m^2 s, $T_{in} = 27$ °C).

at cold wall of outer shell or visualization window. Sometimes, it makes clear observation difficult with disturbance wave described in Fig. 14a. The picture of figure (a) as a result of present visualization work shows the characteristic flow structure of annular channel with two liquid films, liquid droplets and disturbance waves. In addition, it is observed that local dryout area in liquid film causing dryout of liquid film resulting in CHF occurrence was formed as shown in Fig. 14b. In annular geometry, CHF occurs when the liquid film on the heated rod dries out while the liquid film still exists on the cold wall. On the other hand, grid effect observations for flow phenomena were performed. Actually, physical understanding of influence of a flow obstacle of rectangular cell (widely used in PWR type nuclear power plants) on flow boiling has not been sufficiently reported yet except for a flow obstacle of circular cell (used in BWR type nuclear power plants) investigated with a focus of not boiling but dryout by Fukano et al. [18]. Fig. 15 shows the flow patterns with heat flux increasing at upper part (downstream) of spacer grid in the location of 1443 mm from the bottom of heated rod in the annular channel. Bubbles come into being circular shape, together grow to big slug and then brake down to several small size bubbles at the upper part of the grid. It is confirmed through the observations that spacer grid contributes the breakup of both liquid film in cold wall and inner liquid film resulting in effective mixing of fluid.

Fig. 16 indicates the overall grid effect in flow bubbles. The size of bubbles is decreased after passing spacer grid. It seems to be due to much faster bubble departures by the fluid mixing effect of grid. In the middle of spacer grid, the bubble size has the maximum. Coalesced bubbles appear on the spacer grid. Due to small space inside spacer grid or between grid and outer channel wall, bubble coalescence increases. This effect is similar to Lie and Lin's [16] results reporting that due to the space limitation in the narrow duct, bubbles are squeezed and deformed, besides, more large bubbles are found resulting from the coalescence of the small bubbles. Otherwise, since grid increases the pressure drop of flow, bubble generation increases locally, in turn, bubble moving speed increases, coalesced large bubbles appears and the more thermal energy from the heated surface can be absorbed. Additionally, this large bubble makes disturbance waves effectively for both liquid films of heated surface and cold wall. As a result of the mixing effect of overall channel of fluid through the grid region, fluid enthalpy mixing can be done and finally the smaller bubbles than before grid can be shown just after grid. Real phenomena like these observations for spacer grid so far are not well shown in the literatures. The results will contribute to the development of heat transfer enhancement devices with observation results of characteristic flow structures of inner liquid film and outer liquid film.

Fig. 16. Effect of spacer grid (bubble size: before grid (3–5 mm bubble diameter in maximum) < in grid (5–9 mm) ≫ after grid (1–3 mm)) ($P = 11.6$ bar, $G = 900$ kg/m^2 s, $\Delta h_i = 30$ kJ/kg).

5. Conclusion

In the present paper, critical heat flux (CHF) experiments of forced convection boiling were performed to investigate the CHF characteristics of a vertical annular channel with one heated rod and four I-type spacer grids without mixing vane for new refrigerant R-134a under outlet pressure of 11.6, 13, 16, and 20 bar, mass fluxes of 100–600 kg/m^2 s, and inlet temperatures of 25–40 °C.

(1) The parametric trend of the CHF data in R-134a show a general agreement with previous understanding in the water.
(2) The comparison between the present results with effect of the flow obstacle enhancing CHF and water data in similar geometry shows R-134a can be a modeling fluid for simulating water CHF in high pressure and high temperature condition even for annular geometry. The difference for both fluids data seems to be due to both out-boundary rectangular channel and spacer grid installed in the experimental test section to give the uniform annular gap for fuel rod during heating and to prevent the rod vibration. The presence of flow obstacles generally increases the CHF.
(3) Previously developed correlations for tube show reasonable agreements with CHF data for annular channel but a shift of distribution with around −50%, in particular 29.2% RMS error in Katto's generalized correlation due to above-mentioned reasons.
(4) Flow patterns near CHF condition in annular geometry at low mass flux having a film-splitting structure of inner liquid film on heated surface and outer liquid film at cold wall of outer shell or visualization window were observed. In particular, dryout patches on inner liquid film playing the important role in CHF occurrence were observed. In addition, the phenomenological role of spacer grid is understood through the observation of whole spacer grid in flow boiling situation. The direct observation of flowing bubble behaviors contributes to enhancing our understanding on the effect of flow obstacles for flow boiling heat transfer and to advanced development of new heat transfer enhancement devices.

Acknowledgements

This work has been supported by Korea Atomic Energy Research Institute (KAERI) through research contract. Special thanks are given to Dr. S.Y. Chun, Dr. S.K. Moon and Thermal-hydraulic Research Team members from KAERI.

References

[1] L.S. Tong, Y.S. Tang, Boiling Heat Transfer and Two-phase Flow, Taylor & Francis, Washington, DC, 1997.
[2] John G. Collier, John R. Thome, Convective Boiling and Condensation, Clarendon Press/Oxford University Press, New York/Oxford, 1994.
[3] S.H. Chang, W.P. Baek, Critical Heat Flux – Fundamentals and Applications, Chungmoongak, Seoul, 1997 (in Korean).
[4] I.L. Pioro, D.C. Groeneveld, S.S. Doerffer, Y. Guo, S.C. Cheng, A. Vasic, Effects of flow obstacles on the critical heat flux in a vertical tube cooled with upward flow of R-134a, Int. J. Heat Mass Transfer 45 (2002) 4417–4433.
[5] X. Cheng, F.J. Erbacher, U. Muller, Critical heat flux in uniformly heated vertical tubes, Int. J. Heat Mass Transfer 40 (1997) 2929–2939.
[6] R.M. Tain, S.C. Cheng, Critical heat flux measurements in a round tube for CFCs and CFC alternatives, Int. J. Heat Mass Transfer 6 (8) (1993) 2039–2049.
[7] S.Y. Ahmad, Fluid to fluid modeling of critical heat flux: a compensated distortion model, Int. J. Heat Mass Transfer 16 (1973) 641–662.
[8] I.L. Pioro, D.C. Groeneveld, et al., Comparison of CHF measurements in R-134a cooled tubes and the water CHF look-up table, Int. J. Heat Mass Transfer 44 (2001) 73–88.
[9] I.C. Bang, S.H. Chang, W.P. Baek, Visualization of the subcooled flow boiling of R-134a in a vertical rectangular channel with an electrically heated wall, Int. J. Heat Mass Transfer 47 (2004) 4349–4363.
[10] C.H. Kim, S.H. Chang, CHF characteristics of R-134a flowing upward in uniformly heated vertical tube, Int. J. Heat Mass Transfer 48 (2005) 2242–2249.
[11] C.H. Kim, I.C. Bang, S.H. Chang, Critical heat flux performance for flow boiling of R-134a in vertical uniformly heated smooth tube and rifled tube, Int. J. Heat Mass Transfer 48 (2005) 2868–2877.

[12] S. Cho, S.-Y. Chun, M.-K.Chung, W.-P. Baek, Spacer grid effects in an annulus geometry during reflood, NTHAS4, 2004.
[13] R.W. Bowring, A simple but accurate round tube uniform heat flux, dry-out correlation over the pressure range, 0.7–12 MN/m^2 (100–2500 psia), AEEW-R789, 1972.
[14] Y. Katto, H. Ohno, An improved version of the generalized correlation of critical heat flux for the forced convective boiling in uniformly heated vertical tubes, Int. J. Heat Mass Transfer 27 (1984) 1641–1648.
[15] S.Y. Chun, H.J. Chung, S.D. Hong, S. K Yang, M.K. Chung, Critical heat flux in uniformly heated vertical annulus under a wide range of pressures −0.57 to 1.50 MPa, J. Korean Nucl. Soc. 32 (2) (2000) 128–141.
[16] Y.M. Lie, T.F. Lin, Subcooled flow boiling heat transfer and associated bubble characteristics of R-134a in a narrow annular duct, Int. J. Heat Mass Transfer 49 (2006) 2077–2089.
[17] Y.M. Lie, T.F. Lin, Saturated flow boiling heat transfer and associated bubble characteristics of R-134a in a narrow annular duct, Int. J. Heat Mass Transfer 48 (2005) 5602–5615.
[18] T. Fukano, S. Mori, S. Akamatsu, A. Baba, Relation between temperature fluctuation of a heating surface and generation of drypatch caused by a cylindrical spacer in a vertical boiling two-phase upward flow in a narrow annular channel, Nucl. Eng. Des. 217 (2002) 81–90.